Eur. J. Mineral.
2019, **31**, 823–836
Published online 14 June 2019

To Christian Chopin, for 30 years of dedicated service to EJM

Fluorcarmoite-(BaNa), the first Mg-dominant mineral of the arrojadite group

Fernando CÁMARA[1,*], Erica BITTARELLO[2], Marco E. CIRIOTTI[3], Fabrizio NESTOLA[4], Francesco RADICA[5], Federico MASSIMI[6] and Roberto BRACCO[7]

[1]Dipartimento di Scienze della Terra "A. Desio", Università degli Studi di Milano, Via Mangiagalli 34, 20133 Milano, Italy
*Corresponding author, e-mail: fernando.camara@unimi.it
[2]SpectraLab s.r.l. – Spin-off accademico dell'Università degli Studi di Torino, Frazione Cappellazzo 84, 12062 Cherasco (CN), Italy
[3]Associazione Micromineralogica Italiana, Via San Pietro 55, 10073 Devesi-Cirié, Torino, Italy
[4]Dipartimento di Geoscienze, Università degli Studi di Padova, Via Giovanni Gradenigo 6, 35131 Padova, Italy
[5]Dipartimento di Scienze, Università degli Studi Roma Tre, largo San Leonardo Murialdo 1, 00146 Roma, Italy
[6]Dipartimento di Ingegneria Meccanica e Industriale, Università degli Studi Roma Tre, Via della Vasca Navale 79, 00146 Roma, Italy
[7]Associazione Micromineralogica Italiana, Via Montenotte18/6, 17100, Savona, Italy

Abstract: Fluorcarmoite-(BaNa), ideally $^{A1}Ba^{A2}\square\ ^{B1,2}Na^{Na1,2}Na_2^{Na3}\square^{Ca}Ca^{M}Mg_{13}Al(PO_4)_{11}(PO_3OH)^{W}F_2$, was found in a pebble of the riverbed of the upper Maremola Creek, close to the village of Isallo, in the Magliolo municipality (Savona, Liguria, Italy). The root-name is after Monte Carmo di Loano, the highest peak in the area, namesake of the tectonic unit where the mineral was found and the first locality where phosphate mineralization has been found in the region. The mineral is associated with quartz and almandine and has microscopic inclusions of fluorapatite and possible graftonite. It occurs as yellow–orange and translucent crystals in an anhedral centimetric nodule embedded in quartz. Fluorcarmoite-(BaNa) is brittle, and no cleavage or parting was observed. It has a yellow–orange streak, a vitreous lustre, does not fluoresce under shortwave or longwave ultraviolet light and is weakly pleochroic (light yellow). Fluorcarmoite-(BaNa) is optically biaxial positive, with α = 1.6240(5), β = 1.6255(5), γ = 1.6384(5) (589 nm), $2V_{meas}$ = 35(2)° and $2V_{calc}$ = 37.9°. Raman spectroscopy shows the presence of weak bands in the OH-stretching region. The average chemical composition is (wt%, wavelength-dispersive-mode electron microprobe): Na_2O 5.83, K_2O 0.36, CaO 2.64, SrO 0.46, BaO 7.12, MnO 2.01, FeO 17.68, MgO 15.12, Al_2O_3 2.57, P_2O_5 44.96, F 2.14, –O = F_2 0.90, H_2O_{calc} 0.33, total 100.32. The empirical formula calculated on the basis of 50 O + F + (OH) atoms per formula unit (*apfu*), is: $(Na_{3.77}Ca_{0.94}Ba_{0.93}K_{0.15}Sr_{0.09}\square_{0.12})_{\Sigma=6.00}(Mg_{7.52}Fe^{2+}_{4.93}Mn^{2+}_{0.57})_{\Sigma=13.02}Al_{1.01}(PO_4)_{11}(PO_3)(OH_{0.74}F_{0.26})F_2$. Strongest lines in the X-ray powder diffraction pattern are [*d* in Å (I_{calc}) *hkl*]: 4.959 (25) 020, 4.524 (20) 114, 3.188 (28) 206, 3.012 (100) 42$\bar{4}$, 2.735 (32) 60$\bar{2}$, 2.682 (39) 226, 2.526 (25) 424. The crystal structure has been refined using single-crystal X-ray diffractometer data (R_{int} = 4.1%) in space group *Cc* (no. 14) to R_1 = 0.0342 for 11 511 reflections with $F_o > 4\sigma|F|$ and 0.0417 for all 13 232 data. Refined unit-cell parameters are: *a* = 16.4013(3) Å, *b* = 9.9487(1) Å, *c* = 24.4536(8) Å, β = 105.725(2)°, *V* = 3840.80(15) Å^3 (*Z* = 4). Fluorcarmoite-(BaNa) is the first Mg-dominant mineral of the arrojadite group. Mg orders preferentially in the *M*1, *M*2b, *M*3a,b, *M*4a,b and *M*7a,b sites whereas the non-dominant Fe^{2+} and very minor Mn^{2+} show site preference for *M*2a, *M*5a,b and *M*6a,b. The *A*1 site is mostly populated by Ba, the *A*2 site is empty, and minor Fe^{2+} occurs at the B1b site. A significant, but not dominant occupancy of the *Na*3 site by Na is also observed. Only Ca and Al are present at the *Ca* and *Al* sites, respectively. The type material is deposited in the mineralogical collection of the Museo Regionale di Scienze Naturali di Torino, Sezione di Mineralogia, Petrografia e Geologia, Torino (Italy). The mineral and its name have been approved by the IMA-CNMNC (2015-062).

Key-words: arrojadite-group minerals; fluorcarmoite-(BaNa); crystal structure, new mineral; new mineral; phosphate; Monte Carmo; Italy.

1. Introduction

Arrojadite-group minerals occur typically as primary minerals in granitic pegmatites. They are frequent in Lithium–Cesium–Tantalum (LCT) pegmatites belonging to the beryl-"columbite"-phosphate subtype (in the classification of Černý & Ercit, 2005), *e.g.* Eagle *et al.* (2015), Vignola *et al.* (2016) and Birch (2018). Arrojadite-group minerals occur also associated with quartz related to hydrothermal activity accompanying a high-phosphorus, extremely fractionated topaz–"zinnwaldite" leucogranite in the Gemerská Poloma area (Košice Region, Slovak Republic; Števko *et al.*, 2015, 2018). Arrojadite-group minerals are also reported in sedimentary rocks, as in northwestern

0935-1221/19/0031-2868 $ 6.30
https://doi.org/10.1127/ejm/2019/0031-2868

Yukon Territory, Canada (Robertson, 1982; Young & Robertson, 1984; Robinson *et al.*, 1992; Tomes *et al.*, 2018), although this is a unique locality.

The space group of dickinsonite was given by Wolfe (1941) as *C*2/*c*. The space group *C*2/*m* was chosen for arrojadite from the Nickel Plate mine (South Dakota, USA) by Lindberg (1950) and later as $A2_1/n$ by Fisher (1965). The structure of arrojadite-group minerals was first determined on a sample from the Nickel Plate mine (Keystone, South Dakota) by Krutik *et al.* (1979) using the space group *B*2/*b*, a further choice of the space group 15 by Merlino *et al.* (1981) as *C*2/*c*, Moore *et al.* (1981) as *A*2/*a* and Demartin *et al.* (1996) as *C*2/*c*.

The crystal-chemistry of the arrojadite group was reinvestigated by Cámara *et al.* (2006) and Chopin *et al.* (2006), who described the structure in the non-centrosymmetric space group *Cc* and established a new classification scheme for the group based on the general formula $A_2B_2CaNa_{2+x}M_{13}Al(PO_4)_{11}(PO_3OH_{1-x})W_2$, where: A corresponds to large divalent cations (Ba, Sr, Pb) or monovalent cations (K, Na) (*A*1 site), and to monovalent cations (Na) or vacancies (*A*2 site); B corresponds to small divalent cations (Fe, Mn, Mg at the *B*1b and *B*1c sites) and vacancies or monovalent Na cations (at the *B*1 and *B*2 sites); Ca is dominant (with minor Sr) at the *Ca* site; Na is dominant at the *Na*1 and *Na*2 sites; Na can also occupy the site *Na*3 if the third proton bonded to the acid phosphate group is not present ($x = 1$); *M* sites contain small divalent cations (Fe^{2+}, Mn^{2+} and Mg, with minor Li and Zn); the *Al* site can host Fe^{3+} and very minor amounts of Ti and Sc; the *W* site may be occupied by OH or F. The mineral species of the group are then named by a root name plus three suffixes written within parentheses as extended Levinson modifiers and eventual prefixes. The root name is defined by the dominant divalent cation at the *M* sites: arrojadite (Fe), dickinsonite (Mn), and in case of Mg dominance at *M* sites, a further root-name was foreseen by Chopin *et al.* (2006). Regarding suffixes, following the rule of the dominant species of the dominant valence state, the first regards the dominance at the *A*1 site (once Ca sites have been filled by Ca and divalent cations of increasing radius; the second is based on the occupancy of *B* sites, which will depend on the excess at the *M* sites ($^{M}Fe^* = Fe^{2+} + Mn^{2+} + Mg + Zn + Li - 13 = \Sigma M^{2+} + Li - 13$), and will be the dominant cation at the *M* sites or Na in the case that $^{M}Fe^* \leq 0.5$ *pfu*; the third suffix is used when *x* in the above formula is >0.5, meaning that the proton of the acid phosphate group is substituted by another ion (usually Na). Regarding prefixes, these are used when there is an anion substitution at the *W* sites (for instance, "fluor" if (OH) is substituted by F) and/or if there is a substitution of Al by Fe^{3+} at the *Al* sites. After the classification of Chopin *et al.* (2006), two further members of the arrojadite group have been described: arrojadite-(BaNa) (Vignola *et al.*, 2016) and fluorarrojadite-(BaNa) (Ševko *et al.*, 2018).

Fluorcarmoite-(BaNa) is the first arrojadite-group mineral in which Mg is dominant at the *M* sites. Therefore, because Mg > Fe and >Mn, a new root name is warranted according to the nomenclature of the arrojadite group (Chopin *et al.*, 2006). The new root-name is after Monte Carmo di Loano (Savona, Liguria, Italy), the locality where the sample was found. Monte Carmo is the highest peak in the area, and the first locality where phosphate mineralization was found in the region. The prefix "fluor" and suffix -(BaNa) follow the rules in Chopin *et al.* (2006), with an ideal formula $^{A1}Ba^{A2}\square^{B1,2}Na^{Na1,2}Na_2^{Na3}\square^{Ca}Ca^{M}Mg_{13}Al(PO_4)_{11}(PO_3OH)^{W}F_2$ and charge arrangement #3 of Chopin *et al.* (2006). The new mineral was approved by the International Mineralogical Association Commission on New Minerals, Nomenclature and Classification (IMA 2015-062). A fragment of the holotype material is deposited in the mineralogical collection of the Museo Regionale di Scienze Naturali di Torino, Sezione di Mineralogia, Petrografia e Geologia, via Giovanni Giolitti 36, I-10123 Torino (Italy), catalogue number M/15940.

2. Geological setting and mineral occurrence

The mineral occurs in the riverbed of the upper Maremola Creek, close to the village of Isallo, in the Magliolo municipality (Savona, Liguria, Italy; ~44°11′37″N, ~8°15′1″E). The locality is also known by mineral collectors as "Costa Balzi Rossi", after the overlying cliff where rich associations of rare-earth minerals have been found in recent years.

The Monte Carmo tectonic unit of the Briançonnais domain crops out in the area and includes a Permian metavolcanic basement ("*Scisti di Gorra*" schists, "*Porfiroidi del Melogno*" ignimbrites, "*Formazione di Eze*" volcanic ash), followed by a Permo-Triassic cover starting with polygenic conglomerates ("*Verrucano Brianzonese*") and sedimentary quartzites ("*Quarziti di Ponte di Nava*"), underlying younger carbonate sequences. Fluorcarmoite-(BaNa) was found in an erratic rounded pebble in the riverbed of the Maremola Creek by one of the authors (RB) in 2012. The erratic pebble is related to phosphate-bearing quartzites occurring in the area, especially on nearby Monte Carmo di Loano (Boiteau, 1971; Cortesogno, 1984; Menardi Noguera, 1984; Cortesogno *et al.*, 1987; Bracco & Marchesini, 2016), which in turn are part of a thick horizon of quartzites sparsely occurring all over the Alpine range. The origin of phosphate mineralization is uncertain. At the Monte Carmo di Loano site, as well as most other Alpine localities, lazulite is the most widespread phosphate, but several less common phosphates have been reported (Bracco *et al.*, 2007; Bracco & Marchesini, 2016). The mineral is associated with quartz and almandine and has microscopic inclusions of fluorapatite and possible graftonite.

Other minerals found at the same locality, but not associated with fluorcarmoite-(BaNa), are: "adularia", aeschynite-(Y), albite, allanite-(Ce), anatase, bastnäsite-(Ce), brookite, cassiterite, cerussite, chernovite-(Y), churchite-(Y), clinochlore, fergusonite-(Y), gorceixite, goyazite, graftonite, hematite, hingganite-(Y), hundolmenite-(Y), jarosite, lazulite, magnetite, mitridatite, monazite-(Ce),

monazite-(La), paraniite-(Y), pyrite, pyrrothite, rhabdophane-(Nd), rutile, schorl–dravite tourmaline series, thortveitite, titanite, wulfenite and xenotime-(Y) (Bracco *et al.*, 2006, 2007, 2009, 2012; Castellaro, 2014; Bracco & Marchesini, 2016).

Fluorcarmoite-(BaNa), except for minor fluorapatite and possible graftonite inclusions, is the main phosphate observed in the type specimen and occurs as an anhedral centimetric nodule embedded in quartz, presumably syngenetic. Another arrojaditic phosphate of a different composition is associated with fluorcarmoite-(BaNa), but its volume is very small, and it will probably be impossible to characterize it. Its composition is much richer in Ca.

The occurrence strongly resembles that of the type locality of arrojadite-(BaFe) at Alpe Groppera in the Central Alps, Sondrio Province, Lombardy, Italy (Demartin *et al.*, 1996; Cámara *et al.*, 2006; Chopin *et al.*, 2006).

Fig. 1. Photograph of fluorcarmoite-(BaNa). Collection and photo R. Bracco (field of view 25 mm).

3. Appearance and physical properties

Fluorcarmoite-(BaNa) occurs as subhedral equant crystals, stout, more or less platy prisms 10–15 mm in size (Fig. 1) on compact quartz. The mineral is brittle, and no cleavage or parting was observed. Elastic modulus and hardness were measured with a Nano Indenter Agilent G200 in CSM mode (Continuous Stiffness Measurement; Oliver & Pharr 1992, 2004), with a frequency of 45 Hz, amplitude of oscillation 2 nm, constant strain rate of 0.05 s^{-1}; the range of displacement into surface for the average values elastic modulus and hardness is 50–100 nm. Results of hardness and modulus profiles are: elastic modulus 147 ± 3.6 (GPa), hardness 12.12 ± 0.47 (GPa), Vickers hardness 1236, Mohs > 7 < 8. These values were obtained after averaging over five different tests. The Poisson's ratio is assumed to be 0.2. Before and after the tests on the samples, tests on a standard sample of silica were done to calibrate the instrument.

Fluorcarmoite-(BaNa) has a yellow–orange streak, a vitreous lustre and does not fluoresce under shortwave or longwave ultraviolet light. Individual crystals are yellow–orange in colour and translucent. Fluorcarmoite-(BaNa) is optically biaxial positive, with a $2V_{meas}$ = 35(2)° (program ExcalibrW was used to process the extinction data and to determine the $2V$ value; Gunter *et al.*, 2005) and $2V_{calc}$ = 37.9°. The measured refractive indices are α = 1.6240(5), β = 1.6255(5), γ = 1.6384(5) (589 nm). Refractive indices were determined by the double-variation method (Su *et al.*, 1987; Gunter *et al.*, 2005) using standard Cargille liquids as reference. Fluorcarmoite-(BaNa) is weakly pleochroic (light yellow to colourless).

Fluorcarmoite-(BaNa) is unreactive and insoluble in either 2 M HCl, 10% HCl or 65% HNO_3. The measured density of is 3.40 g/cm^3 (Clerici solution). The calculated density obtained from the empirical formula and unit-cell parameters of the single crystal used for the crystal-structure determination is 3.394 g/cm^3. The mean refractive index n of fluorcarmoite-(BaNa), the calculated density and the empirical formula obtained by electron microprobe (see below) yielded a Gladstone-Dale compatibility index (Mandarino, 2007) of 0.020, rated as excellent.

4. Chemical data

4.1. Electron microprobe

The chemical composition was determined using a Cameca SX-50 electron microprobe operated in wavelength-dispersive (WDS) mode at CNR-IGG of Padova (installed at Department of Geosciences of University of Padova) on grains extracted from the holotype, close to the place where the crystal used for the diffraction study was extracted, embedded in epoxy resin and polished. Major and minor elements were determined at 15 kV accelerating voltage and 10 nA beam current (beam size 3 μm), with 40–20 s count time on both peak and background. Probe standards (spectral line; analysing crystal) were: Amelia albite (Na$K\alpha$; TAP), orthoclase (K$K\alpha$; PET), diopside (Ca$K\alpha$; PET), celestine (Sr$L\alpha$; PET), baryte (Ba$L\alpha$; LIF), $MnTiO_3$ (Mn$K\alpha$; LiF), Fe_2O_3 (Fe$K\alpha$; LiF), MgO (Mg$K\alpha$; TAP), Al_2O_3 (Al$K\alpha$; TAP), apatite (P$K\alpha$; TAP), fluorite (F$K\alpha$; TAP). X-ray counts were converted to oxide wt% using the PAP correction program (Pouchou & Pichoir, 1984, 1985). The crystals selected for study are compositionally homogeneous. Only sporadic inclusions of fluorapatite and possible graftonite were found in the sample. H_2O was calculated on the basis of 3(OH) + F groups *pfu* (Chopin *et al.*, 2006). The average of 15 analyses is given in Table 1. The amount of P_2O_5 analysed is higher than expected for 12 P *apfu*. In fact, the normalized values lead to 12.27 P *apfu*. This can be due just to intrinsic uncertainty that in the case of *ca.* 2% in P stoichiometry converts into 1.35 charge, *i.e.*, more than a complete heterovalent substitution on any site. As a matter of fact these deviations from the ideal P content affect low-charge cation contents in a way that may prevent a correct classification (Chopin *et al.*, 2006). In the case of normalization to 12 P *pfu* (and H by charge balance), the

Table 1. Analytical data (wt%) for fluorcarmoite-(BaNa) (15 analytical points).

	Mean	Range	*SD*
Na_2O	5.83	5.48–6.18	0.16
K_2O	0.36	0.30–0.45	0.05
CaO	2.64	2.53–2.79	0.08
SrO	0.46	0.20–0.64	0.13
BaO	7.12	6.14–8.07	0.55
MnO	2.01	1.69–2.33	0.18
FeO	17.68	16.90–18.09	0.29
MgO	15.12	14.84–15.46	0.19
Al_2O_3	2.57	2.48–2.76	0.09
P_2O_5	44.96	43.51–45.29	0.42
F	2.14	2.02–2.29	0.00
Subtotal	100.89	98.10–102.18	0.98
O≡F	0.90	0.85–0.97	0.03
H_2O**	0.33	0.27–0.40	0.04
Total	100.32	96.26–101.65	1.43
P_2O_5*	42.53	41.77–43.05	0.37

*Reduced to the 95% to obtain 12 P *apfu* following recommendations in Chopin *et al.* (2006), see text.
**By stoichiometry.

effect of small P errors on the sums of cations, and therefore on the number of vacancies, is amplified. Normalization using the analysed value produces a sum of *M* sites (Fe^{2+} + Mn^{2+} + Mg) of 12.58 *apfu*. Whereas this could be in agreement with the observed light site scattering at *M* sites (see structure refinements results ahead), it would imply no Fe^{2+} left to be partitioned in *B*1 sites, in contrast with results from refinement. Therefore, following recommendation by Chopin *et al.* (2006), a lower value of P_2O_5 was calculated and used to calculate the normalized mean analysis. Calculated value is reported in Table 1. The empirical formula calculated on the basis of 50 O + F+(OH) *apfu* is then: $(Na_{3.77}Ca_{0.94}Ba_{0.93}K_{0.15}Sr_{0.09}\square_{0.12})_{\Sigma=6.00}(Mg_{7.52}Fe^{2+}_{4.93}Mn^{2+}_{0.57})_{\Sigma=13.02}Al_{1.01}(PO_4)_{11}(PO_3)(OH_{0.74}F_{0.26})F_2$. The simplified formula is $BaNa_4CaMg_{13}Al[(PO_4)_{11}(OH)(PO_3)]F_2$, which requires Na_2O 6.92, BaO 8.56, CaO 3.13, MgO 29.26, Al_2O_3 2.85, P_2O_5 47.55, F 2.12, H_2O 0.50, total 100 wt%.

5. Micro-Raman spectroscopy

The Raman spectrum of fluorcarmoite-(BaNa) (Fig. 2) was obtained using a micro/macro Jobin Yvon Model LabRam HRVIS, equipped with a motorized *x*–*y* stage and an Olympus microscope. The backscattered Raman signal was collected with a 50× objective and the Raman spectrum was obtained for a randomly oriented crystal. The 632.8 nm line of a He–Ne laser was used as excitation; laser power was controlled by density filters. The minimum lateral and depth resolution was set to a few μm. The system was calibrated using the 520.6 cm^{-1} Raman band of silicon before each experimental session. The spectra were collected with multiple acquisitions (2–6) with single counting times ranging between 20 and 180 s. Spectral manipulation such as baseline adjustment, smoothing and normalization were done using the *LabSpec 5* software package (Horiba Jobin Yvon GmbH, 2004, 2005). After background removal, band-component analysis was done using the Fityk software package (Wojdyr, 2010), which enabled the type of fitting function to be selected and allows specific parameters to be fixed or varied accordingly.

6. X-ray diffraction

Experimental X-ray powder diffraction data were collected using an Oxford Gemini R Ultra diffractometer equipped

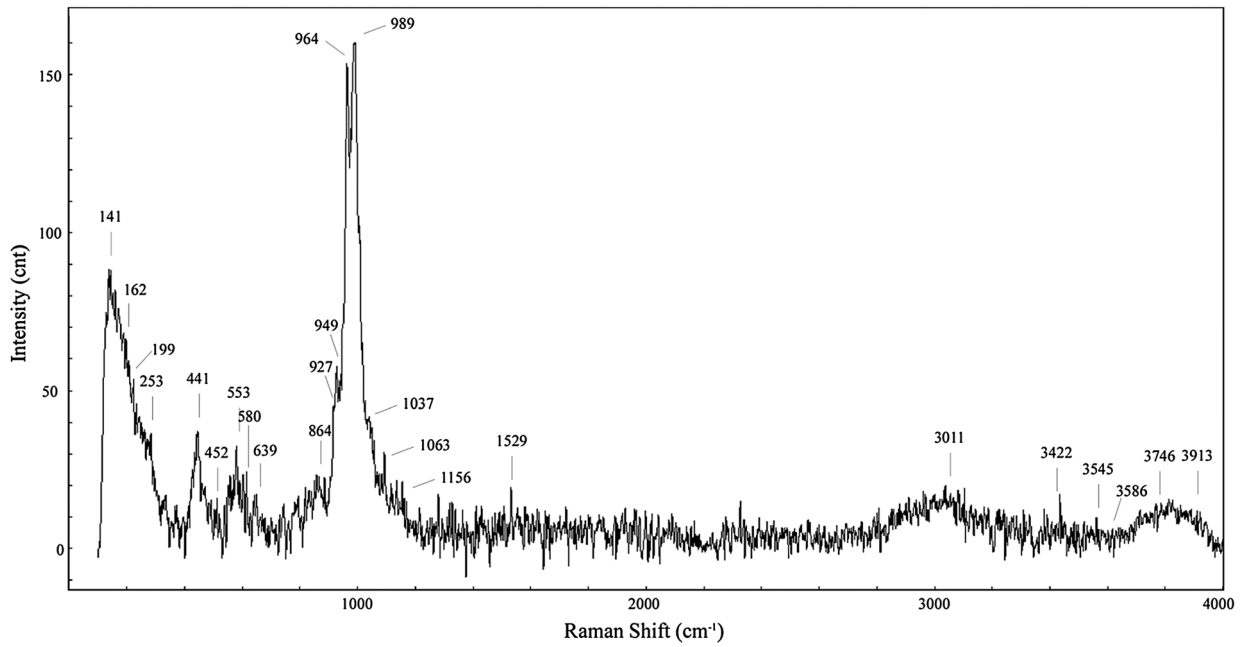

Fig. 2. Raman spectrum of fluorcarmoite-(BaNa) over the 100–4000 cm^{-1} range.

Table 2. X-ray powder diffraction data for fluorcarmoite-(BaNa).*

h	*k*	*l*	d_{obs} (Å)	d_{calc} (Å)	I_{obs}	I_{calc}
1	1	−4	5.182	5.188	11.2	6.3
0	**2**	**0**	**4.959**	**4.974**	**24.8**	**26.1**
3	1	−2	4.733	4.731	12.9	7.3
0	2	2	4.570	4.582	23.8	15.6
1	**1**	**4**	**4.524**	**4.526**	**19.9**	**25.1**
2	2	−2	4.150	4.158	21.7	22.4
1	1	6	3.374	3.374	17.0	22.8
3	1	4	3.289	3.286	10.0	20.2
2	**0**	**6**	**3.188**	**3.186**	**27.5**	**40.3**
2	2	−6	3.097	3.102	19.6	12.3
4	**2**	**−4**	**3.012**	**3.013**	**100.0**	**100.0**
3	3	−2	2.818	2.823	28.4	20.0
3	1	−8	2.808	2.809	17.2	16.9
3	3	0	2.801	2.806	12.7	11.9
1	3	4	2.772	2.777	9.9	9.4
4	0	−8	2.742	2.742	19.8	20.1
6	**0**	**−2**	**2.735**	**2.730**	**32.1**	**27.3**
2	**2**	**6**	**2.682**	**2.683**	**39.2**	**40.3**
1	3	−6	2.567	2.572	11.0	13.8
0	2	8	2.530	2.533	9.2	16.4
4	**2**	**4**	**2.526**	**2.525**	**24.9**	**26.5**
0	4	0	2.480	2.487	9.9	19.5
7	1	−6	2.182	2.180	11.8	12.6
6	4	−2	1.837	1.839	7.0	5.5

*Only reflections with $I_{rel} > 7\sigma(I_{rel})$ are listed.
The seven strongest reflections are reported in bold.

Table 3. Crystal data and summary of parameters describing data collection and refinement for fluorcarmoite-(BaNa).

Crystal system	Monoclinic
Space group	*Cc*
Unit-cell dimensions	
a (Å)	16.4013 (3)
b (Å)	9.9487 (1)
c (Å)	24.4536 (8)
β (°)	105.725 (2)
V (Å^3)	3840.80 (15)
Z	4
F(000)	3616
D_{calc} (g cm^{-3})	3.394
Crystal size (mm)	0.200 × 0.133 × 0.110
Radiation type	Mo*K*α (0.71073 Å)
θ-range for data collection (°)	3.2–32.7
R_{int} (%)	4.1
Reflections collected	48 778
Independent reflections	13 232
$F_o > 4\sigma\|F\|$	11 511
Refinement method	Least-squares, full matrix
No. of refined parameters	847
Final R_{obs} (%) all data	4.17
R_1 (%) $F_o > 4\sigma\|F\|$	3.42
wR_2 (%) $F_o > 4\sigma\|F\|$	8.77
Highest peak/deepest hole (e$^-$ Å^{-3})	1.32/−1.02
Goodness of fit on F^2	1.040

with a CCD area detector at CrisDi (Interdepartmental Centre for the Research and Development of Crystallography, Torino, Italy) with graphite-monochromatized Mo*K*α radiation. The unit-cell parameters refined from the powder data with the software GSAS (Larson & Von Dreele, 1994) are: $a = 16.426(9)$, $b = 9.920(8)$, $c = 24.43(3)$ Å, $\beta = 105.65(11)°$, $V = 3832(6)$ Å^3, $Z = 4$. Fluorcarmoite-(BaNa) is monoclinic, space group *Cc*. Observed *d*-spacings and diffraction intensities for Mo*K*α radiation are compared with those calculated from the structure model using PLATON v-140513 (Spek, 2009) and are reported in Table 2.

Single-crystal X-ray diffraction data were collected on a crystal of 0.200 × 0.133 × 0.110 mm using an Oxford Xcalibur Gemini Ultra diffractometer equipped with a Ruby CCD area detector at CrisDi with graphite-monochromatised Mo*K*α radiation (λ = 0.71073 Å). No crystal twinning was observed. Crystal data and experimental details are reported in Table 3.

The intensities of 48 640 reflections with $-24 \leq h \leq 23$, $-15 \leq k \leq 14$, $-36 \leq l \leq 37$ were collected to 65.5° 2θ using a 1° frame and an integration time of 42 s. Data were integrated and corrected for Lorentz and polarization background effects using the package CrysAlisPro (Agilent Technologies, Version 1.171.36.28, release 01-02-2013 CrysAlis171). Data were corrected for empirical absorption using spherical harmonics, implemented in the SCALE3 ABSPACK scaling algorithm in CrysAlisPro. Refinement of the unit-cell parameters was based on 21 512 measured reflections with $I > 10\sigma(I)$.

At room temperature, the unit-cell parameters are: $a = 16.4013(3)$, $b = 9.9487(1)$, $c = 24.4536(8)$ Å; $\beta = 105.725(2)°$, $V = 3840.80(15)$ Å^3, $Z = 4$, space group *Cc* and $Z = 4$. The *a:b:c* ratio is 1.6486:1:2.4580. The structure was refined starting from the atom coordinates of arrojadite-(KNa) (Cámara *et al.*, 2006) using the SHELX set of programs (Sheldrick, 2008). Structure refinement converged to $R_1 = 0.0342$ for 11 511 reflections with $F_o > 4\sigma|F|$ and 0.0417 for all 13 232 data. Table 4 reports atomic coordinates. Table S1 with anisotropic-displacement parameters is deposited and available as Supplementary Material linked to this article at https://pubs.geoscienceworld.org/eurjmin. Tables 5–7 report selected bond distances, geometrical parameters and bond valence for fluorcarmoite-(BaNa). Site scattering values and site occupancies are reported in Table 8. The CIF and structure factor list are available as part of the Supplementary Material.

7. Results

7.1. Raman spectroscopy

The Raman spectrum of fluorcarmoite-(BaNa) from 100 to 4000 cm^{-1} is reported in Fig. 2. The spectral region between 100 and 700 cm^{-1} includes the phosphate bending modes (PO_4 and $PO_3(OH)$ bending vibrations). Quite intense bands are found at 141, 162, 199 and 253 cm^{-1} and these bands may be simply described as lattice vibrations of phosphate groups. A series of broad bands are observed at 441, 452, 553, 580, 639 cm^{-1} and these bands are attributed to motions of cations at the *M* sites.

The Raman spectrum, in the region of 700–1400 cm^{-1}, shows a number of overlapping bands. Intense Raman bands

Table 4. Atoms, site occupancy (cation sites)/bond valence (B.V., anion sites, valence units, v.u.), fractional atom coordinates (Å), and equivalent isotropic displacement parameters (Å^2) for fluorcarmoite-(BaNa).

	Site occupancy/B.V.	*x*	*y*	*z*	U_{eq}
*A*1	0.964(1) Ba^{2+}	−0.00061(6)	0.50259(2)	−0.24760(4)	0.0196(1)
*A*2	□				
*B*1	0.341(4) Na^{+}	−0.2963(3)	0.5457(5)	−0.04276(17)	0.005*
*B*1b	0.305(4) Fe^{2+}	−0.27827(17)	0.6095(2)	−0.01984(10)	0.0039(6)*
*B*2	0.776(10) Na^{+}	−0.1330(3)	0.4809(4)	−0.11904(18)	0.0212(10)
*B*2b	0.224(10) Na^{+}	−0.1722(8)	0.4809(11)	−0.1085(5)	0.025*
*Na*1	0.957(7) Na^{+}	0.0001(4)	0.0004(5)	0.0019(2)	0.0256(5)
*Na*2	0.902(10) Na^{+}	0.1365(4)	0.5184(4)	0.12220(18)	0.0436(18)
*Na*3	0.189(13) Na^{+}	−0.503(4)	0.434(2)	−0.251(2)	0.087(8)*
*Na*3x	0.490(14) Na^{+}	−0.5117(8)	0.5265(10)	−0.2572(5)	0.080(4)*
*Ca*a	0.476(11) Ca^{2+}	−0.2301(3)	0.2164(4)	0.01924(19)	0.0196(12)
*Ca*b	0.524(11) Ca^{2+}	−0.2647(3)	0.2739(4)	−0.0099(2)	0.0323(18)
*M*1	0.901(10) Mg^{2+} 0.099(10) Fe^{2+}	−0.22094(19)	0.8968(3)	0.02817(14)	0.0402(10)
*M*2a	0.415(11) Mg^{2+} 0.585(11) Fe^{2+}	−0.28937(11)	0.48449(15)	−0.23009(7)	0.0154(5)
*M*2b	0.608(11) Mg^{2+} 0.392(11) Fe^{2+}	0.28804(12)	0.51569(16)	0.23472(7)	0.0099(5)
*M*3a	0.948(13) Mg^{2+}	−0.10801(18)	−0.0172(2)	−0.13771(11)	0.0061(7)
*M*3b	0.853(11) Mg^{2+} 0.147(11) Fe^{2+}	0.10671(17)	1.0161(2)	0.14227(10)	0.0139(7)
*M*4a	0.784(9) Mg^{2+} 0.216(9) Fe^{2+}	−0.02111(14)	0.25170(19)	0.09941(8)	0.0101(6)
*M*4b	0.731(9) Mg^{2+} 0.269(9) Fe^{2+}	0.02022(13)	0.74906(19)	−0.09528(8)	0.0121(6)
*M*5a	0.409(9) Mg^{2+} 0.591(9) Fe^{2+}	0.03343(9)	0.25408(14)	−0.09790(6)	0.0118(4)
*M*5b	0.487(9) Mg^{2+} 0.513(9) Fe^{2+}	−0.03480(9)	0.74488(15)	0.10222(6)	0.0087(4)
*M*6a	0.335(10) Mg^{2+} 0.665(10) Fe^{2+}	−0.20437(10)	0.70445(16)	0.15000(6)	0.0163(5)
*M*6b	0.456(10) Mg^{2+} 0.544(10) Fe^{2+}	−0.29668(10)	0.79640(16)	−0.14510(6)	0.0128(5)
*M*7a	0.634(9) Mg^{2+} 0.366(9) Fe^{2+}	−0.28167(12)	0.2057(2)	−0.15412(7)	0.0139(5)
*M*7b	0.635(10) Mg^{2+} 0.365(10) Fe^{2+}	−0.21956(12)	0.7051(2)	−0.34102(7)	0.0154(6)
Al	0.974(5) Al^{3+}	−0.0008(2)	0.5006	0.00249(14)	0.0067(2)
*P*1	0.683(6) P	−0.1147(2)	1.0122(3)	0.13417(13)	0.0099(4)
*P*1′	0.317(6) P	−0.0813(4)	1.0027(6)	0.1677(3)	0.0113(14)*
*P*1b	0.341(4) P	−0.4199(4)	0.4987(5)	−0.1621(3)	0.0104(12)
*P*1b′	0.659(4) P	−0.3860(2)	0.4873(3)	−0.12899(14)	0.012*
*P*2a	1 P	−0.13074(13)	0.4654(2)	0.07934(8)	0.0105(3)
*P*2b	1 P	0.12912(13)	0.53436(19)	−0.07444(8)	0.0102(3)
*P*3a	1 P	−0.12832(12)	0.74790(18)	−0.03701(7)	0.0087(3)
*P*3b	1 P	−0.37395(13)	0.75144(18)	0.04174(7)	0.0088(3)
*P*4a	1 P	−0.10290(13)	0.23166(19)	−0.04659(7)	0.0101(3)
*P*4b	1 P	0.10175(12)	0.76840(19)	0.05087(8)	0.0096(3)
*P*5a	1 P	0.12927(12)	0.72937(18)	0.21506(7)	0.0087(3)
*P*5b	1 P	−0.12978(13)	0.27178(18)	−0.21020(8)	0.0110(3)
*P*6a	1 P	0.14374(13)	0.30126(19)	0.20779(8)	0.0118(4)
*P*6b	1 P	−0.14466(12)	0.69881(17)	−0.20344(8)	0.0093(3)
O1a	1 O/1.91	−0.4762(4)	0.4312(5)	−0.1302(2)	0.0148(10)
O1b	1 O/1.94	−0.0258(3)	0.0676(5)	0.1344(2)	0.0144(10)
O2a	1 O/2.00	−0.3906(4)	0.6368(5)	−0.1347(3)	0.0171(11)
O2b	1 O/1.91	−0.1107(4)	0.8612(5)	0.1400(3)	0.0156(11)
O3a	1 O/2.24	0.3576(5)	0.5772(6)	0.1802(3)	0.050(2)
O3b′	0.659(4) O/1.14	−0.3204(4)	0.4535(6)	−0.0725(2)	0.013*
O3bx	0.341(4) O/0.46	−0.4705(6)	0.5264(8)	−0.2220(4)	0.0104(15)*
O4a	1 O/1.63	−0.1813(5)	1.0365(8)	0.0777(4)	0.080(2)
O4x	1 O/1.93	−0.3478(3)	0.4139(5)	−0.1711(2)	0.0175(9)
O5a	1 O/2.08	−0.0512(3)	0.4413(5)	0.0572(2)	0.0107(10)

(Continued on next page)

Table 4. (Continued)

	Site occupancy/B.V.	*x*	*y*	*z*	U_{eq}
O5b	1 O/2.10	0.0492(4)	0.5595(5)	−0.0542(2)	0.0115(10)
O6a	1 O/1.94	−0.1188(4)	0.5985(5)	0.1132(3)	0.0179(11)
O6b	1 O/2.05	0.1188(4)	0.4054(5)	−0.1071(3)	0.0200(12)
O7a	1 O/1.99	−0.1297(4)	0.3408(5)	0.1168(2)	0.0133(10)
O7b	1 O/1.95	−0.3725(4)	0.1573(5)	−0.1137(2)	0.0163(11)
O8a	1 O/2.00	−0.2107(4)	0.4578(7)	0.0314(3)	0.0294(14)
O8b	1 O/2.02	−0.2895(4)	1.0322(5)	−0.0259(2)	0.0174(11)
O9a	1 O/1.96	−0.0839(4)	0.8319(5)	−0.0747(2)	0.0144(10)
O9b	1 O/2.09	−0.4141(3)	0.6695(5)	0.0794(2)	0.0116(9)
O10a	1 O/2.05	−0.0953(4)	0.6046(5)	−0.0339(2)	0.0142(10)
O10b	1 O/1.96	0.0957(3)	0.3982(5)	0.0391(2)	0.0094(9)
O11a	1 O/2.03	−0.1096(4)	0.8119(6)	0.0225(2)	0.0160(11)
O11b	1 O/1.92	−0.3933(4)	0.6880(5)	−0.0176(2)	0.0148(11)
O12a	1 O/1.85	−0.2242(4)	0.7459(6)	−0.0619(2)	0.0172(11)
O12b	1 O/1.97	−0.2759(4)	0.7532(5)	0.0660(3)	0.0167(11)
O13a	1 O/2.12	−0.0445(3)	0.3568(5)	−0.0471(2)	0.0122(10)
O13b	1 O/1.95	0.0460(3)	0.6445(5)	0.0516(2)	0.0103(10)
O14a	1 O/2.12	−0.0651(4)	0.1261(5)	−0.0791(2)	0.0141(11)
O14b	1 O/2.14	0.0654(3)	0.8720(5)	0.0845(2)	0.0124(10)
O15a	1 O/1.91	−0.0951(4)	0.1840(5)	0.0142(2)	0.0162(11)
O15b	1 O/1.94	0.0959(4)	0.8146(6)	−0.0090(2)	0.0182(12)
O16a	1 O/2.09	−0.1937(4)	0.2652(5)	−0.0755(2)	0.0167(11)
O16b	1 O/1.89	0.1949(3)	0.7356(6)	0.0815(2)	0.0163(11)
O17a	1 O/1.96	0.0481(3)	0.6765(5)	0.1738(2)	0.0128(10)
O17b	1 O/1.99	−0.0487(4)	0.3254(6)	−0.1695(3)	0.0172(11)
O18a	1 O/1.97	0.1330(4)	0.3242(6)	−0.2255(2)	0.0182(12)
O18b	1 O/2.01	−0.1322(4)	0.3217(6)	−0.2693(2)	0.0125(10)
O19a	1 O/1.99	0.1332(4)	0.8822(5)	0.2127(2)	0.0219(13)
O19b	1 O/1.88	−0.1324(4)	0.1155(5)	−0.2076(2)	0.0189(13)
O20a	1 O/2.04	0.2063(3)	0.6719(6)	0.1976(2)	0.0155(11)
O20b	1 O/2.06	−0.2064(4)	0.3280(5)	−0.1915(2)	0.0172(11)
O21a	1 O/1.89	0.0577(3)	0.3462(5)	0.1690(2)	0.0116(10)
O21b	1 O/1.95	−0.0614(4)	0.6510(6)	−0.1635(2)	0.0178(11)
O22a	1 O/1.87	0.1487(4)	0.6462(6)	−0.2317(2)	0.0205(13)
O22b	1 O/2.00	−0.1516(4)	0.6463(6)	−0.2622(2)	0.0216(12)
O23a	1 O/2.07	0.1493(4)	0.1487(5)	0.2066(2)	0.0146(10)
O23b	1 O/2.03	−0.1530 (4)	0.8529(5)	−0.2023(2)	0.0175(12)
O24a	1 O/1.96	0.2172(4)	0.3620(6)	0.1875(3)	0.0198(12)
O24b	1 O/1.87	−0.2197(4)	0.6392(6)	−0.1823(2)	0.0183(12)
*W*1	1 F/0.68	−0.2314(3)	1.0010(5)	−0.13727(17)	0.0238(10)
*W*2	1 F/0.71	−0.2711(4)	0.4906(6)	0.1416(3)	0.0460(16)

*The temperature factor has the form $\exp(-T)$ where $T = 8(\pi^2)U(\sin(\theta)/\lambda)^2$ for isotropic atoms.

are observed at 989 and 964 cm^{-1} with shoulder bands at 949, 927 and 864 cm^{-1}. These bands are assigned to the PO_4 v_1 symmetric stretching modes. The Raman band at 989 cm^{-1} is attributed to the stretching vibrations of $PO_3(OH)$ groups. Multiple bands are observed depending upon to which cation the phosphate is bonding. Raman shoulder bands are also observed at 1037, 1063 and 1156 cm^{-1} and these are assigned to the PO_4 v_3 antisymmetric stretching modes (Casciani & Condrate, 1980; Frost *et al.*, 2013).

In the region of 1800–4000 cm^{-1}: broad bands and weak shoulders are observed. Band component analysis enables resolution with bands at 3011, 3422, 3545, 3586, 3746 and 3913 cm^{-1} that might be assigned to OH stretching modes. However, the stretching modes described by Cámara *et al.* (2006), Frost *et al.* (2013) and Della Ventura *et al.* (2014) are a doublet centred at *ca.* 3526 and 3554 cm^{-1}. Weak components at 3100–3200 cm^{-1} are reported by Frost *et al.* (2013) and by Della Ventura *et al.* (2014) and can be interpreted as due to the O3x–H3x bonding (mistakenly reported by Della Ventura *et al.* (2014) as O25–H3, as O25*a*,*b* = W1,2 is not involved in the PO_3OH group). The presence of significant scattering at the Na3,3x sites implies that the intensity of that vibration must be weak. It is worth noting that Della Ventura *et al.* (2014) reported the presence of NH_4^+ in arrojadite-(KNa) from Rapid Creek (Yukon) by means of WDS microprobe analysis and FTIR, which would show bands related to ν_3 antisymmetric stretching modes at *ca.* 3090 cm^{-1}. Additional bending ν_4 modes at 1400 cm^{-1} are then expected (found by Della Ventura *et al.*, 2014 at *ca.* 1450 cm^{-1}). The presence of a weak band at 1529 cm^{-1} does not support the presence of NH_4^+ in fluorcarmoite-(BaNa) that could account for the "excess" scattering at the *Na*3,3x sites (see below).

Table 5. The phosphate groups. Main interatomic distances (Å), geometrical parameters and bond valence values[a] (v.u.) for fluorcarmoite-(BaNa).

*P*1–O3a	1.474(7)	0.99	*P*2b–O6b	1.497(6)	1.37	*P*5a–O19a	1.524(6)	1.28
–O2b	1.509(6)	0.91	–O8b	1.528(6)	1.27	–O17a	1.530(5)	1.27
–O4a	1.529(8)	0.86	–O5b	1.542(6)	1.23	–O18a	1.533(6)	1.26
–O1b	1.556(6)	0.81	–O7b	1.551(5)	1.20	–O20a	1.550(5)	1.20
<*P*1–O>	1.517	3.57	<*P*2b–O>	1.530	5.08	<*P*5a–O>	1.534	5.01
V[b] (Å^3)	1.78	1.78		*V*(Å^3)	1.83		*V*(Å^3)	1.85
*P*1′*–O3a	1.346(9)	0.64	*P*3a–O10a	1.520(5)	1.30	*P*5b–O18b	1.520(5)	1.30
–O1b	1.520(8)	0.42	–O12a	1.525(6)	1.28	–O17b	1.526(6)	1.28
–O2b	1.580(8)	0.36	–O11a	1.540(5)	1.23	–O20b	1.553(6)	1.19
<*P*1′–O>	1.482	1.41	–O9a	1.562(6)	1.17	–O19b	1.557(5)	1.18
			<*P*3a–O>	1.537	4.98	<*P*5b–O>	1.539	4.95
*P*1b–O3bx	1.502(11)	0.46	*V*(Å^3)	1.86		*V*(Å^3)	1.87	
–O1a	1.517(8)	0.44						
–O4x	1.517(8)	0.44	*P*3b–O9b	1.509(6)	1.33	*P*6a–O23a	1.522(5)	1.29
–O2a	1.547(7)	0.41	–O11b	1.534(6)	1.25	–O21a	1.538(5)	1.24
<*P*1b–O>	1.520	1.76	–O10b	1.538(5)	1.24	–O24a	1.546(7)	1.22
V(Å^3)	1.79		–O12b	1.557(6)	1.18	–O22a	1.551(5)	1.20
			<*P*3b–O>	1.534	5.01	<*P*6a–O>	1.539	4.95
*P*1b′–O2a	1.495(6)	0.91	*V*(Å^3)	1.85		*V*(Å^3)	1.87	
–O4x	1.527(6)	0.84						
–O3b′	1.541(7)	0.81	*P*4a–O16a	1.503(6)	1.35	*P*6b–O22b	1.503(69	1.35
–O1a	1.574(7)	0.75	–O15a	1.533(6)	1.26	–O21b	1.524(6)	1.28
<*P*1b′–O>	1.534	3.31	–O14a	1.544(5)	1.22	–O23b	1.540(5)	1.23
V(Å^3)	1.84		–O13a	1.573(5)	1.14	–O24b	1.574(6)	1.13
			<*P*4a–O>	1.538	4.97	<*P*6b–O>	1.535	5.01
*P*2a–O8a	1.506(6)	1.34	*V*(Å^3)	1.86		*V*(Å^3)	1.85	
–O7a	1.538(5)	1.24						
–O6a	1.546(5)	1.22	*P*4b–O15b	1.512(6)	1.32			
–O5a	1.561(5)	1.17	–O14b	1.536(6)	1.25			
<*P*2a–O>	1.538	4.97	–O13b	1.538(6)	1.24			
V(Å^3)	1.851		–O16b	1.543(6)	1.23			
			<*P*4b–O>	1.532	5.04			
			V(Å^3)	1.84				

[a]Bond-valence parameters from Gagné & Hawthorne (2015) for bond with $O^{=}$ and from Brown (1981) for bonds with F^{-}.
[b]The fourth oxygen could not be identified in the Fourier-difference map and was not added to the model; bond valence at split sites *P*1 and *P*1′ and *P*1b and *P*1b′ correspond to the partial occupancies at these sites.
**V* = polyhedral volume.

7.2. Description of the structure

The crystal structure of fluorcarmoite-(Ba,Na) is topologically identical to the structure of arrojadite-(KNa): four-, five- and six coordinated cations are linked by (PO_4) groups and Al octahedra sharing apices, except for *M*4a,b and *M*5a, b that share an edge with *P*2a,b and *P*4a,b, respectively – in fact these cation polyhedra show the highest angle-variance values (σ^2, Tables 5 and 6) along with *P*1 sites. Interestingly, site-scattering refinement (Hawthorne *et al.*, 1995) shows the highest scattering for the *M*5a,b and *M*6a,b sites, indicating that Fe^{2+} orders preferentially in these sites (Table 4).

From the point of view of the Structure Hierarchy Hypothesis (Hawthorne, 1983, 1994), "*structures may be ordered hierarchically according to the polymerization of coordination polyhedra of higher bond valence*". Therefore, higher bond-valence polyhedra polymerize to form homo- or heteropolyhedral clusters; these may be considered as the fundamental building block (FBB) of the structure. The FBB is repeated (often polymerized) by symmetry to form the structural unit, a complex (usually anionic) polyhedral array (not necessarily connected). In the case of arrojadite minerals, we can identify the FBB as the complex polyanion $M_{12}O_{17}(OH,F)_6[PO_4]_{10}^{6-}$ (Fig. 3a). It is composed of two elements that repeat twice in the FBB: a folded strip of four edge-sharing octahedra and one edge-sharing PO_4 group and a strip of two edge-sharing octahedra plus an edge sharing PO_4 group (Fig. 3b). Furthermore, six PO_4 group link the strip by sharing their vertices. The $M_{12}O_{17}(OH,F)_6[PO_4]_{10}^{6-}$ unit repeats along [010] by sharing the (OH,F) anions with the adjacent units, forming a column of the form $M_{12}O_{17}(OH,F)_6[PO_4]_{10}^{6-}$. Within the (010) plane, these columns link by sharing (OH,F) anions and vertices of PO_4 tetrahedra, plus other (PO_4) and (AlO_6) groups, as well as the *M*1 tetrahedron. Monovalent and divalent alkaline-earth cations occur in the interstitial voids as well as within the columns. There are four $M_{12}O_{17}(OH,F)_6[PO_4]_{10}^{6-}$ per unit cell.

The structure (Fig. 4) shows disorder at alkali sites and *P*1 sites, which have been modelled as split sites, following Cámara *et al.* (2006). The refinement converged to a 1/3:2/3 population, not compatible with a missing centre of

Table 6. The *Al* and *M* sites. Main interatomic distances (Å), geometrical parameters and bond valence values[a] (v.u.) for fluorcarmoite-(BaNa).

Al–O5a	1.850(6)	0.573	*M*3b–O14b	1.997(6)	0.425	*M*6a–O18b	2.024(5)	0.450
–O10a	1.875(6)	0.538	–W2	2.024(7)	0.311	–O12b	2.126(6)	0.356
–O5b	1.884(6)	0.525	–O23a	2.026(6)	0.398	–O6a	2.138(5)	0.346
–O13a	1.886(5)	0.523	–O19a	2.126(6)	0.318	–O2b	2.249(6)	0.268
–O10b	1.891(5)	0.516	–O9b	2.127(6)	0.317	–O24a	2.364(7)	0.206
–O13b	1.892(5)	0.515	–O1b	2.191(6)	0.275	–W2	2.377(6)	0.142
<*Al*–O>	1.880	3.190	<*M*3b–O>	2.082	2.044	<*M*6a–O>	2.213	1.767
V(Å^3)*	8.83		*V*(Å^3)	11.83		*V*(Å^3)	13.99	
*M*1–O4a	1.843(10)	0.597	*M*4a–O1b	2.032(6)	0.397	*M*6b–O18a	2.011(6)	0.454
–O8b	2.005(6)	0.414	–O21a	2.063(5)	0.370	–O12a	2.120(6)	0.354
–O12b	2.040(6)	0.383	–O9b	2.111(6)	0.332	–O6b	2.158(6)	0.324
–O11a	2.051(7)	0.374	–O7a	2.132(6)	0.317	–O2a	2.273(6)	0.249
–O12a	2.654(7)	0.096	–O5a	2.143(5)	0.309	–W1	2.284(5)	0.177
<*M*1–O>	2.119	1.864	–O15a	2.212(6)	0.265	–O24b	2.343(6)	0.212
V(Å^3)	7.35		<*M*4a–O>	2.115	1.990	<*M*6b–O>	2.198	1.770
			V(Å^3)	12.03		*V*(Å^3)	13.74	
*M*1–O2b	2.862(7)							
			*M*4b–O1a	2.011(6)	0.419	*M*7a–O22a	2.020(6)	0.420
*M*2a–O4x	2.061(5)	0.388	–O21b	2.077(6)	0.361	–O7b	2.056(6)	0.387
–O24b	2.077(6)	0.374	–O9a	2.078(7)	0.360	–O20b	2.110(6)	0.343
–O23a	2.079(5)	0.373	–O5b	2.130(5)	0.320	–O16a	2.151(6)	0.312
–O19a	2.089(6)	0.364	–O7b	2.135(6)	0.317	–W1	2.194(5)	0.209
–O20b	2.114(6)	0.344	–O15b	2.236(5)	0.252	–O4x	2.322(5)	0.212
<*M*2a–O>	2.084	1.843	<*M*4b–O>	2.111	2.029	<*M*7a–O>	2.142	1.884
V(Å^3)	6.27		*V*(Å^3)	11.92		*V*(Å^3)	12.62	
*M*2b–O23b	2.051(6)	0.388	*M*5a–O17b	2.025(6)	0.423	*M*7b–O22b	2.034(6)	0.408
–O3a	2.068(6)	0.373	–O2a	2.082(6)	0.372	–O7a	2.067(6)	0.378
–O24a	2.073(6)	0.369	–O6b	2.108(5)	0.351	–O16b	2.113(6)	0.341
–O20a	2.092(6)	0.354	–O11b	2.110(5)	0.349	–O20a	2.118(6)	0.337
–O19b	2.097(6)	0.350	–O14a	2.202(6)	0.284	–W2	2.120(6)	0.256
<*M*2b–O>	2.076	1.833	–O13a	2.255(6)	0.252	–O3a	2.491(7)	0.145
V(Å^3)	6.41		<*M*5a–O>	2.130	2.031	<*M*7b–O>	2.157	1.865
						V(Å^3)	12.86	
*M*3a–O14a	2.009(6)	0.404	*M*5b–O17a	2.021(5)	0.422			
–O23b	2.020(6)	0.395	–O6a	2.072(6)	0.376			
–W1	2.035(6)	0.291	–O2b	2.089(6)	0.362			
–O19b	2.110(6)	0.322	–O11a	2.111(6)	0.345			
–O9a	2.111(6)	0.321	–O14b	2.208(6)	0.277			
–O1a	2.181(6)	0.274	–O13b	2.275(5)	0.238			
<*M*3a–O>	2.078	2.007	<*M*5b–O>	2.129	2.021			
V(Å^3)	11.73		*V*(Å^3)	12.11				

[a]Bond-valence parameters from Gagné & Hawthorne (2015) for bond with $O^{=}$ and from Brown (1981) for bonds with F^{-}.
**V* = polyhedral volume.

symmetry as proposed by other authors (Kallfaß *et al.*, 2010; Vignola *et al.*, 2016). It seems therefore that the apparent presence of a centre of symmetry in some other localities is the result of local disorder due to high-temperature crystal growth. The shape of the electron density at some anion sites is oblate and represents local disorder associated with complex cation order. In particular, disorder is present at *Na*3 and *Na*3x, but chemical composition implies that the overall cation occupancy of the *Na*3 cavity is <0.5 *apfu*, and thus the third modifier is not required for naming. Consequently, the occupancy of H3x is reduced and explains – along with the fluorine content – the weak bands observed in the OH-stretching region of the Raman spectrum.

Using the chemical analysis and the observed site scattering, it is also possible to assign ions to specific sites (Table 8). The agreement is very good. The incident bond-valence in Table 4 validates the model. Anions at the *W*1 and *W*2 sites show incident bond-valence <1 valence units (v.u.) characteristic of F^{-} ions or (OH) groups. The other anion sites are O3b′ and O3bx, which are two split sites related to the disorder of the *P*1 sites and to the partial occupancy of the *Na*3 site by Na and K (or H in case of vacancy at the *Na*3 site).

In Table 8, the ordering of Fe^{2+} (and Mn^{2+}) is evident, with preference for the distorted *M*2a, *M*5a,b as well as the more regular but still larger *M*6a,b sites. In particular, some Na is disordered over the *M*6a,b and *M*7a,b sites, in agreement with the site scattering as well as mean bond-length. Na can therefore disorder the *inter-column* sites and the octahedra, exchanging with Fe^{2+}. This exchange is probably related to high-temperature crystallization, in

Table 7. The alkali sites. Selected interatomic distances (Å), geometrical parameters and bond valence values[a] (v.u.) for fluorcarmoite-(BaNa).

*A*1–O18b	2.749 (6)	0.264	*B*2b–O10a	2.278 (12)	0.055	*Na*2–O10b	2.296 (6)	0.203
–O18a	2.758 (6)	0.258	–O16a	2.352 (12)	0.046	–O13b	2.317 (7)	0.193
–O22a	2.770 (6)	0.251	–O24b	2.363 (12)	0.045	–O24a	2.362 (7)	0.174
–O22b	2.798 (6)	0.234	–O20b	2.476 (12)	0.034	–O20a	2.428 (7)	0.148
–O17b	2.863 (6)	0.200	–O13a	2.543 (13)	0.029	–O21a	2.591 (8)	0.101
–O17a	2.887 (6)	0.188	–O3b′	2.815 (15)	0.015	–O16b	2.663 (8)	0.085
–O21a	2.898 (5)	0.183	–O4x	2.948 (13)	0.011	–O17a	2.676 (8)	0.082
–O21b	2.919 (6)	0.174	–O21b	3.049 (14)	0.009	–O5a	3.152 (8)	0.026
<*A*1–O>	2.830	1.754	<*B*2b–O>	2.603	0.244	<*Na*2–O>	2.561	1.013
V(Å^3)*	31.59		*V*(Å^3)	26.78		*V*(Å^3)	25.22	
*B*1–O8a	2.154 (7)	0.137	*Ca*–O16b	2.210 (7)	0.215	*Na*3–O3a	2.45 (6)	0.054
–O11b	2.335 (7)	0.089	–O8b	2.223 (7)	0.208	–O1b	2.74 (5)	0.026
–O12a	2.426 (7)	0.072	–O15a	2.274 (7)	0.183	–O4x	2.76 (6)	0.025
–O2a	2.528 (7)	0.056	–O4a	2.296 (9)	0.174	–O1a	2.86 (5)	0.019
–O15b	3.144 (7)	0.013	–O8a	2.430 (8)	0.125	–O23a	3.07 (6)	0.011
<*B*1–O>	2.517	0.368	–O16a	2.590 (7)	0.085	–O23b	3.10 (6)	0.011
V(Å^3)	12.68		–O7a	2.793 (7)	0.052	–O19b	3.17 (5)	0.009
			–O15b	2.917 (8)	0.038	–O19a	3.19 (5)	0.008
*B*1–O3b′	1.170 (7)		<*Ca*–O>	2.467	1.079	<*Na*3–O>	2.92	0.165
			V(Å^3)	25.28		*V*(Å^3)	29.41	
*B*1b–O3b′	2.014 (6)	0.149	*Ca*b–O8a	2.160 (8)	0.264	*Na*3x–O3a	2.495 (13)	0.033
–O12a	2.045 (6)	0.139	–O16a	2.225 (7)	0.225	–O19b	2.735 (15)	0.018
–O11b	2.057 (6)	0.135	–O15b	2.327 (8)	0.175	–O1b	2.760 (13)	0.017
–O8a	2.078 (7)	0.129	–O3b′	2.369 (8)	0.158	–O19a	2.821 (15)	0.015
–O12b	2.533 (6)	0.047	–O8b	2.452 (7)	0.129	–O2b	2.827 (13)	0.015
<*B*1b–O>	2.146	0.598	–O16b	2.526 (7)	0.108	–O4x	3.138 (13)	0.007
V(Å^3)	7.74		–O15a	2.829 (8)	0.051	–O1a	3.148 (13)	0.007
			–O7b	2.913 (7)	0.042	<*Na*3x–O>	2.846	0.113
			<*Ca*b–O>	2.475	1.153	*V*(Å^3)	23.61	
			V(Å^3)	25.32				
*B*2–O13a	2.313 (7)	0.179	*Na*1–O14a	2.342 (8)	0.210	*Na*3x–O3bx	0.939(14)	
–O10a	2.352 (7)	0.163	–O14b	2.385 (7)	0.190	*Na*3–O3bx	1.19 (4)	
–O24b	2.388 (7)	0.150	–O15a	2.473 (8)	0.154			
–O20b	2.398 (7)	0.146	–O15b	2.487 (8)	0.149			
–O21b	2.473 (7)	0.122	–O9a	2.611 (8)	0.111			
–O17b	2.599 (8)	0.091	–O9b	2.638 (8)	0.104			
–O16a	2.703 (7)	0.071	–O11b	2.686 (9)	0.093			
–O5b	3.081 (7)	0.029	–O11a	2.738 (9)	0.082			
<*B*2–O>	2.538	0.951	<*Na*1–O>	2.545	1.091			
V(Å^3)	24.95		*V*(Å^3)	25.09				

[a]Bond-valence parameters from Gagné & Hawthorne (2015) for bond with $O^{=}$ and from Brown (1981) for bonds with F^{-}.
**V* = polyhedral volume; bond valence in split sites (*B*1 and *B*1b, *B*2 and *B*2b, *Ca*a and *Ca*b, *Na*3 and *Na*3x) correspond to the partial occupancies at these sites.

agreement with the split model for *P*1 and some alkali sites. Note that the observed site distribution of Mg and Fe^{2+}(Mn^{2+}) in fluorocarmoite-(NaBa) (Table 8) agrees closely with the site populations of Cámara *et al.* (2006) in samples from Rapid Creek and Horrsjöberg, which have lower Mg (2.69 and 3.61 *apfu*, respectively).

8. Related minerals

Fluorcarmoite-(BaNa), $^{A1}Ba^{A2}\square^{B1,2}Na^{Na1,2}Na_2{}^{Na3}\square\square^{Ca}Ca(Mg,Fe^{2+},Mn^{2+})_{12}Al(PO_4)_{11}(PO_3OH)F_2$, is a new member of the arrojadite group (Table 9). Provided that the environment is low in Fe and Mn, it seems possible to find other members of the arrojadite group with the root-name *carmoite*. The other sample reported in literature with high, but not dominant Mg-content is sample Gentile-154 from Spluga Valley (Lombardy, Italy; Demartin *et al.*, 1996; Chopin *et al.*, 2006), which has up to 5.68 Mg *apfu* (lower than the 8.12 *apfu* of Fe^{2+}, the dominant element). The refinement of Demartin *et al.* (1996) shows Mg ordered preferentially at the *M*1, *M*3 and *M*4 sites, in agreement with the findings of this study for the Mg-dominant end-member.

Nowadays, the structure of phosphates containing large channels is of interest in Material Sciences because of the possibility to use their analogues as feasible novel alkali-metal ion batteries (Trad *et al.*, 2010). In particular, sulphate analogues of alluaudite have been tested and show promising properties (Marinova *et al.*, 2015). Preliminary tests on materials with the arrojadite topology have been done by Kallfaß *et al.* (2011), who described it as a novel cathode material which exhibits an excellent cycle behaviour

Table 8. Site-scattering values* and site occupancies (excluding P sites).

Site	Occupancy	eps (calc)	eps (obs)
*A*1	$(Ba_{0.93}Sr_{0.05})_{\Sigma 0.98}$	54	54.0(8)
*A*2	(□)		
*B*l	$(Na_{0.41}Fe^{2+}_{0.33})_{\Sigma 0.74}$	13.1	11.67(6)
*B*2	$Na_{0.98}$	10.8	11.0(1)
*Na*1	$Na_{0.98}$	10.8	10.6(1)
*Na*2	$Na_{0.85}$	9.4	9.90(1)
*Na*3	$(Na_{0.22}K_{0.15})_{\Sigma 0.37}$	5.3	7.5(1.4)
Ca	$Ca_{0.94}$	18.8	20.0(1)
		Σ 122.2	Σ 124.7
Al	$(Al_{0.97}Fe^{3+}_{0.02}\square_{0.01})_{\Sigma 1}$	13.1	12.7(2)
*M*1	$(Mg_{0.88}Fe^{2+}_{0.12})_{\Sigma 1}$	13.7	13.4(1)
*M*2a	$(Mg_{0.39}Fe^{2+}_{0.61})_{\Sigma 1}$	20.5	20.2(1)
*M*2b	$(Mg_{0.58}Fe^{2+}_{0.42})_{\Sigma 1}$	18.3	17.5(1)
*M*3a	Mg_1	12	11.4(2)
*M*3b	$(Mg_{0.82}Fe^{2+}_{0.18})_{\Sigma 1}$	14.5	14.1(1)
*M*4a	$(Mg_{0.75}Fe^{2+}_{0.24}Mn_{0.01})_{\Sigma 1}$	15.5	15.0(1)
*M*4b	$(Mg_{0.70}Fe^{2+}_{0.29}Mn_{0.01})_{\Sigma 1}$	16.2	15.8(1)
*M*5a	$(Mg_{0.37}Fe^{2+}_{0.61}Mn_{0.02})_{\Sigma 1}$	20.8	20.3(1)
*M*5b	$(Mg_{0.46}Fe^{2+}_{0.52}Mn_{0.02})_{\Sigma 1}$	19.5	19.2(1)
*M*6a	$(Mg_{0.18}Fe^{2+}_{0.74}Mn_{0.25}Na_{0.10})_{\Sigma 1}$	21.7	21.3(1)
*M*6b	$(Mg_{0.29}Fe^{2+}_{0.40}Mn_{0.19}Na_{0.12})_{\Sigma 1}$	20	19.6(1)
*M*7a	$(Mg_{0.55}Fe^{2+}_{0.37}Mn_{0.03}Na_{0.05})_{\Sigma 1}$	17.5	17.1(1)
*M*7b	$(Mg_{0.55}Fe^{2+}_{0.35}Mn_{0.04}Na_{0.06})_{\Sigma 1}$	17.4	17.0(1)
		Σ 240.3	Σ 234.6
		Σ 362.5	Σ 359.3

*In the sense of Hawthorne *et al.* (1995), in electrons per site (eps).

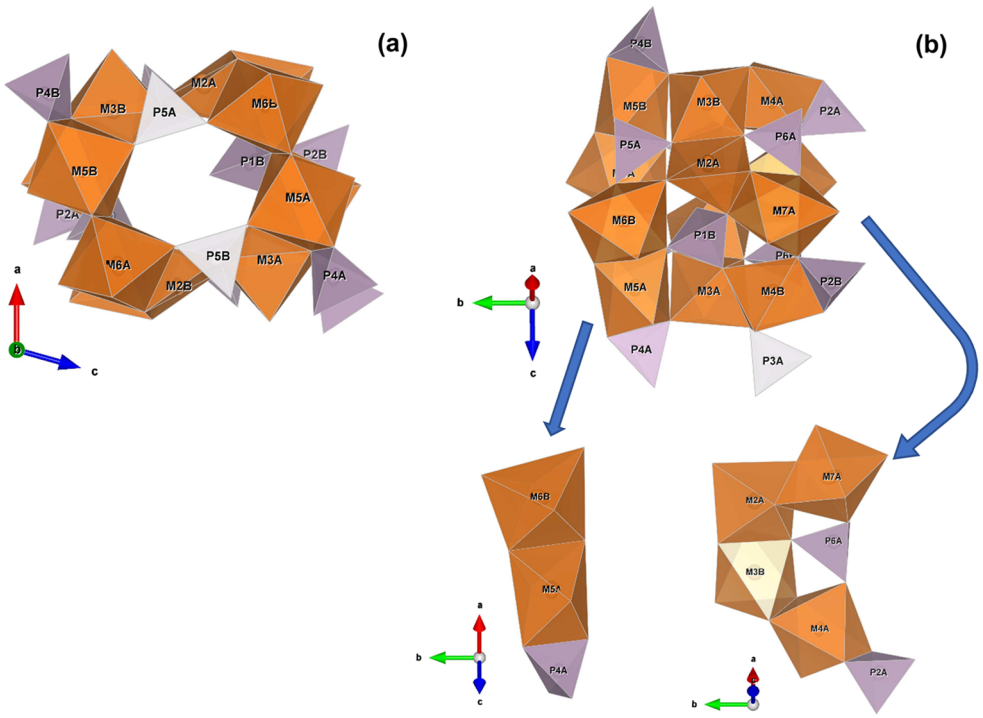

Fig. 3. The $M_{12}O_{17}(OH,F)_6[PO_4]^{6-}_{10}$ unit from [010] (a) and onto (100) (b), with details of the two building strips. *M* sites in orange, *P* sites in violet. Drawing obtained with VESTA 3 (Momma & Izumi, 2011).

Table 9. Arrojadite group. Comparison of three different root-name members of the group.

	Fluorcarmoite-(BaNa)	Arrojadite-(KNa)	Dickinsonite-(KMnNa)
Reference	(1)	(2)	(2)
Ideal formula	$BaNaCaNa_2Mg_{12}Al(PO_4)_{11}(PO_3OH)F_2$	$KNa_3(CaNa_2)Fe^{2+}_{13}Al(PO_4)_{11}(PO_3OH)(OH)_2$	$K(NaMn)CaNa_3AlMn_{13}(PO_4)_{12}(OH)_2$
Crystal system	Monoclinic	Monoclinic	Monoclinic
Space group	*Cc*	*Cc*	*Cc*
a (Å)	16.4013(3)	16.5220(11)	16.6900(9)
b (Å)	9.9487(1)	10.0529(7)	10.1013(5)
c (Å)	24.4536(8)	24.6477(16)	24.8752(13)
β (°)	105.725(2)	106.509(2)	105.616(2)
V (Å^3)	3840.80(15)	3932.2(7)	4038.9(7)
Z	4	4	4
Axial ratios (**a**:**b**:**c**)	1.649:1:2.458	1.643:1:2.452	1.652:1:2.463
D_{meas} (g cm^{-3})	3.40	Unknown	Unknown
D_{calc} (g cm^{-3})	3.394	3.437	3.496
Strongest lines in powder pattern: d_{obs} (Å)(*I*)	3.012(100), 2.682(39), 2.735(32), 2.818(28), 3.188(28), 2.526(25), 4.959(25), 4.570(24), 4.150(22), 4.5242(20)	3.049(100), 2.691(71), 5.861(29), 2.793(28), 5.026(28), 2.798(25), 2.777(24)	3.04(100), 2.717(80), 3.22(60), 2.85(45), 5.93(40), 2.770(40), 2.554(35)
Optical character	Biaxial (+), n_α = 1.6240(5), n_β = 1.6255(5), n_γ = 1.6384(5) (589 nm), $2V_{meas.}$ = 35(2)°, $2V_{calc.}$ = 38°	Biaxial (+), n_α = 1.651(1), n_β = 1.656(1), n_γ = 1.662(10) (589 nm), $2V_{meas.}$ = 87.8(1)°, $2V_{calc.}$ = 85°	Biaxial (+), n_α = 1.658, n_β = 1.662, n_γ = 1.671 (589 nm), $2V_{calc.}$ = 68°
Colour	Yellow–orange	Yellow	Vivid Green
Hardness	7	5	3.5–4
Streak	Yellow–orange	White	White
Luster	Vitreous	Vitreous	Vitreous
Habit and forms	Anhedral crystals	Euhedral platy prismatic	Mica-like platelets
Type locality	"Costa Balzi Rossi", Maremola Creek, Isallo, Magliolo, Savona, Liguria, Italy	Rapid Creek, Dawson mining district, Yukon Territory, Canada	Fillow Quarry, Branchville, Ridgefield, Fairfield County, Connecticut, USA
Associations	Quartz, (fluorapatite, and possible graftonite inclusion)	Euhedral quartz and some "limonite" (former siderite?)	Eosphorite, triploidite, lithiophilite, quartz

References: (1) This study; (2) Cámara *et al.* (2006).

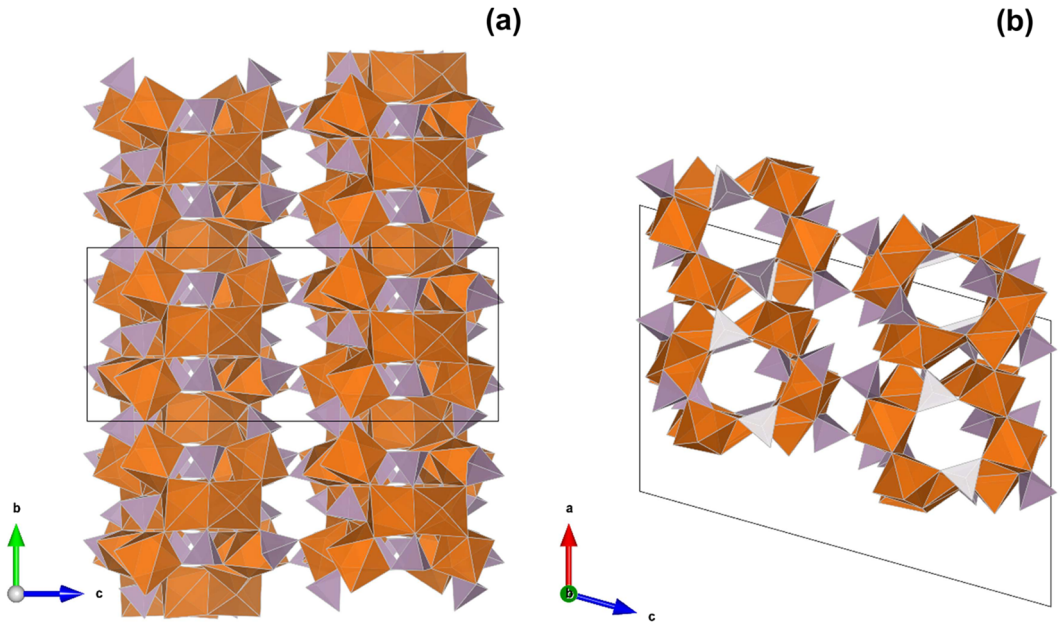

Fig. 4. The four $M_{12}O_{17}(OH,F)_6[PO_4]^{6-}_{10}$ units per unit cell. *P*3a,b and *M*1 tetrahedra, Al octahedra as well as alkaline site atoms have been removed for the sake of simplicity. Colours as in Fig. 3. Drawing obtained with VESTA 3 (Momma & Izumi, 2011).

because lithium content has little effect on its structure stability. The high variability of cation coordination and radius in the arrojadite structure makes it a promising candidate, particularly the Mn-endmember fluordickinsonite-(NaNaNa).

Acknowledgements: FC thanks Christian Chopin for involving him in the study of arrojadites, one of the most complex structures FC has dealt with. The paper benefited from the journal reviews made by Frank C. Hawthorne and an anonymous reviewer, and Guest Editor W. Maresch.

References

Birch, W.D. (2018): Minerals in the arrojadite, alluaudite and jahnsite–whiteite groups from the Mount Wills pegmatite field, Victoria, Australia. *Eur. J. Mineral.*, **30**, 635–645.

Boiteau, A. (1971): Un exemple de la tectonique des Alpes Ligures: la région du M. Carmo (Italie). *Géologie Alpine I*, **47**, 117–132.

Bracco, R. & Marchesini, M. (2016): Le quarziti a lazulite della Liguria e la scoperta della fluorcarmoite-(BaNa). *Micro*, **14**, 68–84.

Bracco, R., Callegari, A., Boiocchi, M., Balestra, C., Armellino, G., Ciriotti, M.E. (2006): Costa Balzi Rossi (Magliolo, Val Maremola, Savona, Liguria): una nuova località per minerali di terre rare e scandio. *Micro*, **4**, 161–178.

Bracco, R., Balestra, C., Odicino, G. (2007): Costa Balzi Rossi e dintorni: un aggiornamento. *Prie – Notiziario Mineral. Ligure*, **3**, 79–97.

Bracco, R., Castellaro, F., Ciuffardi, M., Odicino, G. (2009): Paraniite-(Y) ed altri ritrovamenti da Costa Balzi Rossi. *Prie – Notiziario Mineral. Ligure*, **5**, 61–75.

Bracco, R., Balestra, C., Castellaro, F., Mills, S.J., Ma, C., Callegari, A.M., Boiocchi, M., Bersani, D., Cadoni, M., Ciriotti, M.E. (2012): Nuovi minerali di Terre Rare da Costa Balzi Rossi, Magliolo (SV), Liguria. *Micro*, **10**, 66–77.

Brown, I.D. (1981): The bond-valence method: an empirical approach to chemical structure and bonding – Structure and bonding in crystals. Academic Press, New York, NY 1–30.

Cámara, F., Oberti, R., Chopin, C., Medenbach, O. (2006): The arrojadite enigma: I. A new formula and a new model for the arrojadite structure. *Am. Mineral.*, **91**, 1249–1259.

Casciani, F.S. & Condrate, R.A. (1980): The infrared and Raman spectra of several calcium hydrogen phosphates. *in* "Proceedings – International Congress on Phosphorus Compounds, 2nd (1980)", 175–190.

Castellaro, F. (2014): Chernovite-(Y) a Costa Balzi Rossi. Segnalazioni in breve. *Prie*, **10**, 46.

Černý, P. & Ercit, S. (2005): The classification of granitic pegmatites revisited. *Can. Mineral.*, **43**, 2005–2026.

Chopin, C., Oberti, R. & Cámara, F. (2006): The arrojadite enigma: II. Compositional space, new members and nomenclature of the group. *Am. Mineral.*, **91**, 1260–1270.

Cortesogno, L. (1984): Metamorfismo e magmatismo prealpini nel basamento e nel tegumento delle Alpi Liguri. *Mem. Soc. Geol. Ital.*, **28**, 79–94. (in Italian).

Cortesogno, L., Galbiati, B., Principi, G. (1987): Note alla "Carta geologica delle ofioliti del Bracco" e ricostruzione della paleogeografia Giurassico-Cretacica. *Ofioliti*, **12**, 261–342.

Della Ventura, G., Bellatreccia, F., Radica, F., Chopin, C., Oberti, R. (2014): The arrojadite enigma III. The incorporation of volatiles: a polarised FTIR spectroscopy study. *Eur. J. Mineral.*, **26**, 679–688.

Demartin, F., Gramaccioli, C.M., Pilati, T., Sciesa, E. (1996): Sigismundite, $(Ba,K,Pb)Na_3(Ca,Sr)(Fe,Mg,Mn)_{14}Al(OH)_2(PO_4)_{12}$, a new Ba-rich member of the arrojadite group from Spluga Valley, Italy. *Can. Mineral.*, **34**, 827–834.

Eagle, R.M., Birch, W.D., McKnight, S. (2015): Phosphate minerals in granitic pegmatites from the Mount Wills district, North-Eastern, Victoria. *Proc. R. Soc. Vic.*, **127**, 55–68.

Fisher, D.J. (1965): Dickinsonites, fillowite and alluaudites. *Am. Mineral.*, **50**, 1647–1669.

Frost, R.L., Xi, Y., Scholz, R., Horta, L.F.C. (2013): The phosphate mineral arrojadite-(KFe) and its spectroscopic characterization. *Spectrochim. Acta A*, **109**, 138–145.

Gagné, O.C. & Hawthorne, F.C. (2015): Comprehensive derivation of bond-valence parameters for ion pairs involving oxygen. *Acta Crystallogr. B*, **71**, 562–578.

Gunter, M.E., Downs, R.T., Bartelmehs, K.L., Evans, S.H., Pommier, C.J.S., Grow, J.S., Sanchez, M.S., Bloss, F.D. (2005): Optic properties of centimeter-sized crystals determined in air with the spindle stage using EXCALIBRW. *Am. Mineral.*, **90**, 1648–1654.

Hawthorne, F.C. (1983): Graphical enumeration of polyhedral clusters. *Acta Crystallogr. A*, **39**, 724–736.

— (1994): A bond-topological approach to theoretical mineralogy: crystal structure, chemical composition and chemical reactions. *Phys. Chem. Minerals*, **39**, 841–874.

Hawthorne, F.C., Ungaretti, L., Oberti, R. (1995): Site populations in minerals; terminology and presentation of results of crystal-structure refinement. *Can. Mineral.*, **33**, 907–911.

Horiba Jobin Yvon GmbH (2004, 2005): *LabSpec [Software for Raman spectroscopic data analysis, acquisition and manipulation]*. Version 5.64.15.

Kallfaß, C., Hoch, C., Schier, H., Simon, A., Schubert, H. (2010): The transition metal-rich orthophosphate arrojadite with special structural features. *Z. Naturforsch B*. **65b**, 1427–1433.

Kallfaß, C., Hoch, C., Schier, H., Wituchowski, C., Görke, O., Schubert, H. (2011): The ortho-phosphate arrojadite as a new material for cathodes in Li-ion batteries. *in* "Materials Challenges in Alternative and Renewable Energy: Ceramic Transactions", G. Wicks, J. Simon, R. Zidan, E. Lara-Curzio, T. Adams, J. Zayas, A. Karkamkar, R. Sindelar & B. Garcia-Diaz, eds. John Wiley & Sons Inc, Hoboken, NJ, USA.

Krutik, V.M., Pushcharovskii, D.Y., Pobedimskaya, E.A., Belov, N.V. (1979): Crystal structure of arrojadite. *Kristallografiya*, **24**, 743–750.

Larson, A.C. & Von Dreele, R.B. (1994): *General Structure Analysis System (GSAS)*. Los Alamos National Laboratory Report LAUR. 86–748.

Lindberg, M.L. (1950): Arrojadite, hühnerkobelite, and graftonite. *Am. Mineral.*, **35**, 59–76.

Mandarino, J.A. (2007): The Gladstone-Dale compatibility of minerals and its use in selecting mineral species for further study. *Can. Mineral.*, **45**, 1307–1324.

Marinova, D., Kostov, V., Nikolova, R., Kukeva, R., Zhecheva, E., Sendova-Vasileva, M., Stoyanova, R. (2015): From kröhnkite- to alluaudite-type of structure: novel method of synthesis of sodium manganese sulfates with electrochemical properties in alkali-metal ion batteries. *J. Mater. Chem. A*, **3**, 22287–22299.

Menardi Noguera, A. (1984): Nuove osservazioni sulla struttura del Massiccio del Monte Carmo (Alpi Liguri). *Boll. Soc. Geol. Ital.*, **103**, 189–203.

Merlino, S., Mellini, M., Zanazzi, P.F. (1981): Structure of arrojadite, $KNa_4CaMn_4Fe_{10}Al(PO_4)_{12}(OH,F)_2$. *Acta Crystallogr. B*, **37**, 1733–1736.

Momma, K. & Izumi, F. (2011): VESTA 3 for three dimensional visualization of crystal, volumetric and morphology data. *J. Appl. Crystallogr.*, **44**, 1272–1276.

Moore, P.B., Araki, T., Merlino, S., Mellini, M., Zanazzi, P.F. (1981): The arrojadite-dickinsonite series, $KNa_4Ca(Fe,Mn^{2+})_{14}Al(OH)_2(PO_4)_{12}$: crystal structure and crystal chemistry. *Am. Mineral.*, **66**, 1034–1049.

Oliver, W.C. & Pharr, G.M. (1992): An improved technique for determining hardness and elastic modulus using load and displacement sensing indentation experiments. *J. Mater. Res.*, **7**, 1564–1583.

—, — (2004): Measurement of hardness and elastic modulus by instrumented indentation: Advances in understanding and refinements to methodology. *J. Mater. Res.*, **19**, 3–20.

Pouchou, J.L. & Pichoir, F. (1984): A new model for quantitative analysis: Part I. Application to the analysis of homogeneous samples. *La Recherche Aérospatiale*, **3**, 13–38.

—, — (1985): 'PAP' φ(ρZ) procedure for improved quantitative microanalysis. *in* "Microbeam Analysis", J.T. Armstrong, ed. San Francisco Press, San Francisco, CA, USA, 104–106.

Robertson, B.T. (1982): Occurrence of epigenetic phosphate minerals in a phosphatic iron-formation, Yukon Territory. *Can. Mineral.*, **20**, 177–187.

Robinson, G.W., Van Velthuizen, J., Ansell, H.G., Sturman, B.D. (1992): Mineralogy of the Rapid Creek and Big Fish River area, Yukon Territory. *Mineral. Rec.*, **23**, 1–47.

Sheldrick, G.M. (2008): A short history of SHELX. *Acta Crystallogr. A*, **64**, 112–122.

Smith, D.G.W. & Nickel, E.H. (2007): A system for codification for unnamed minerals: report of the Subcommittee for Unnamed Minerals of the IMA Commission on New Minerals, Nomenclature and Classification. *Can. Mineral.*, **45**, 983–1055.

Spek, A.L. (2009): Structure validation in chemical crystallography. *Acta Crystallogr. D*, **65**, 148–155.

Števko, M., Uher, P., Sejkora, J., Malíková, R., Škoda, R., Vaculovič, T. (2015): Phosphate minerals from the hydrothermal quartz veins in specialized S-type granites, Gemerská Poloma (Western Carpathians, Slovakia). *J. Geosci.*, **60**, 237–249.

Števko, M., Sejkora, J., Uher, P., Cámara, F., Škoda, R., Vaculovič, T. (2018): Fluorarrojadite-(BaNa), $BaNa_4CaFe_{13}Al(PO_4)_{11}(PO_3OH)F_2$, a new member of the arrojadite group from Gemerská Poloma, Slovakia. *Mineral. Mag.*, **82**, 863–876.

Strunz, H. & Nickel, E.H. (2001): Strunz Mineralogical Tables. Chemical Structural Mineral Classification System, 9th edition. E. Schweizerbart, Stuttgart, Germany, 870 p.

Su, S.C., Bloss, F.D., Gunter, M.E. (1987): Procedures and computer programs to refine the double variation method. *Am. Mineral.*, **72**, 1011–1013.

Tomes, H.E., Di Cecco, V.E., Tait, K.T., Cámara, F. (2018): Crystal structure of near-endmember Arrojadite-(BaNa) from Big Fish River, Yukon, Canada. *Can. Mineral.*, **56**, 1–16.

Trad, K., Carlier, D., Croguennec, L., Wattiaux, A., Ben Amara, M., Delmas, C. (2010): $NaMnFe_2(PO_4)_3$ alluaudite phase: synthesis, structure, and electrochemical properties as positive electrode in lithium and sodium batteries. *Chem. Mater.*, **22**, 5554–5562.

Vignola, P., Hatert, F., Baijot, M., Dal Bo, F., Andò, S., Bersani, D., Pavese, A., Risplendente, A., Vanini, F. (2016): Arrojadite-(BaNa), $BaNa_3(Na,Ca)Fe^{2+}_{13}Al(PO_4)_{11}(PO_3OH)(OH)_2$, a new phosphate mineral from the Luna albite pegmatite, Dorio commune, Lecco Province, Italy. *Can. Mineral.*, **54**, 1021–1032.

Wojdyr, M. (2010): Fityk: a general-purpose peak fitting program. *J. Appl. Crystallogr.*, **43**, 1126–1128.

Wolfe, C.W. (1941): The unit cell of dickinsonite. *Am. Mineral.*, **26**, 338–342.

Young, F.G. & Robertson, B.T. (1984): The Rapid Creek Formation: An Albian flysch-related phosphatic iron formation in northern Yukon Territory. *Can. Soc. Pet. Geol. Special Publ. – Mem.*, **9**, 361–372.

Received 4 March 2019
Modified version received 2 May 2019
Accepted 3 May 2019